Chemical Science

EDGE ARTICLE

View Article Online
View Journal | View Issue

Cite this: *Chem. Sci.*, 2019, **10**, 7816

All publication charges for this article have been paid for by the Royal Society of Chemistry

Received 11th May 2019
Accepted 3rd July 2019

DOI: 10.1039/c9sc02314c

rsc.li/chemical-science

Near-infrared fluorescein dyes containing a tricoordinate boron atom†

Naoki Ando,[a] Hiroki Soutome[a] and Shigehiro Yamaguchi *[ab]

Bora-fluoresceins (**BF**s), fluorescein analogues containing a tricoordinate boron atom instead of an oxygen atom at the 10-position of the fluorescein skeleton, were synthesized as a new family of fluorescein analogues. The deprotonated **BF**s exhibited absorption and fluorescence in the near-infrared region, which were significantly red-shifted relative to those of hitherto-known heteroatom-substituted fluorescein analogues on account of the orbital interaction between the tricoordinate boron atom and the fluorescein skeleton. **BF**s also showed multi-stage changes resulting from a Lewis acid–base equilibrium at the boron center in combination with a Brønsted acid–base equilibrium at the phenolic hydroxy group.

Introduction

Xanthene is one of the most representative π-conjugated scaffolds for fluorescent dyes, exemplified by fluoresceins and rhodamines. A variety of xanthene-based fluorescence probes have so far been developed and applied to the visualization of various biological events by fluorescence imaging.[1–9] These dyes typically exhibit absorption and fluorescence in the visible region. To increase their practical utility in current biological applications, xanthene dyes exhibiting long-wavelength absorption and emission, particularly in the near-infrared (NIR) region, remain attractive target compounds. The use of NIR light entails several advantages, *e.g.*, deep tissue penetration, photo-toxicity mitigation, suppression of auto-fluorescence interference, and evasion of cross-talk with conventional fluorescence probes emitting in the visible region in multi-color imaging.[10–15]

In the development of NIR-emissive xanthene dyes, a variety of structural modifications have been explored extensively. A typical approach is the π-expansion of the xanthene skeleton. For instance, naphthofluoresceins, where the fluorescein skeleton is extended with two naphthalene moieties, present absorption and emission in the red-to-NIR region (Fig. 1a).[16–20] Alternatively, the replacement of the endocyclic oxygen atom at the 10-position of the xanthene skeleton with other heteroatoms represents an effective approach to achieve longer-wavelength absorption and emission. A series of xanthene dyes containing various main-group elements, including group 14,[21–29] 15,[30–34] and 16 [35–42] elements, have been synthesized and their properties have been investigated. Nevertheless, boron-containing xanthene dyes have not received much attention to date. Recently, borinate-substituted xanthene dyes have been reported independently by Egawa and Stains (Fig. 1b).[43,44] However, these studies remain limited to tetracoordinate

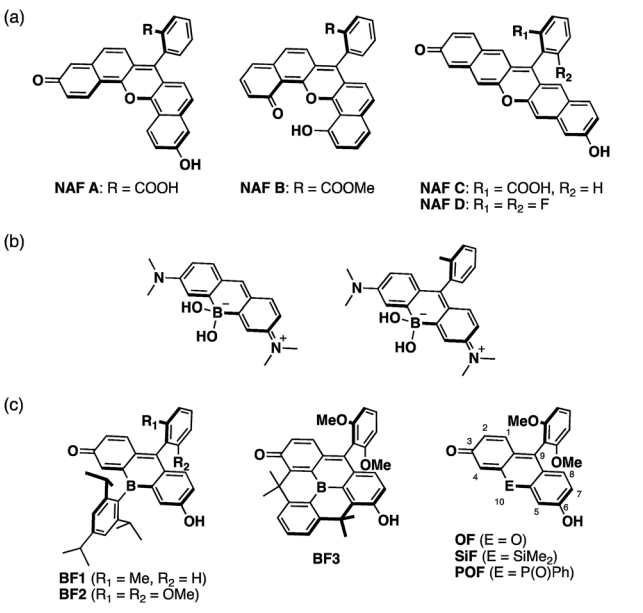

Fig. 1 Molecular structures of (a) naphthofluoresceins, (b) previously reported borinate-substituted xanthene dyes, and (c) bora-fluoresceins and their analogues studied in this work. An overview of the numbering of the fluorescein skeleton is also depicted.

[a]*Department of Chemistry, Graduate School of Science, Integrated Research Consortium on Chemical Sciences (IRCCS), Nagoya University, Furo, Chikusa, Nagoya 464-8602, Japan. E-mail: yamaguchi@chem.nagoya-u.ac.jp*

[b]*Institute of Transformative Bio-Molecules (WPI-ITbM), Nagoya University, Furo, Chikusa, Nagoya 464-8602, Japan*

† Electronic supplementary information (ESI) available: Experimental procedures, spectral data, details of the computational studies, and crystallographic data for **BF2** and **BF3**. CCDC 1913398 and 1913399. For ESI and crystallographic data in CIF or other electronic format see DOI: 10.1039/c9sc02314c

boron-containing derivatives. Our motivation was to prepare the missing part of the heteroatom-substituted xanthene dyes, *i.e.*, tricoordinate boron-containing fluoresceins.

A tricoordinate boron atom introduced into the π-conjugated system should perturb the electronic structure through orbital interaction between the vacant p orbital on the boron atom and the π* orbital of the π-skeleton (p–π* interaction).[45–54] As target compounds, we designed bora-fluoresceins **BF1–3**, which contain a tricoordinate boron atom at the 10-position of the fluorescein skeleton (Fig. 1c). Herein, we disclose that these bora-fluoresceins exhibit significantly red-shifted absorption and emission as well as unusual multi-stage responses to Brønsted and Lewis bases. The impact of the boron atom on these properties will be discussed in this article.

Results and discussion

The key step in the synthetic route to bora-fluoresceins **BF1–3** (Scheme 1) is the synthesis of boron-substituted dihydroxyxanthone precursor **4**. While other heteroatom-substituted dihydroxyxanthones have been synthesized *via* the introduction of hydroxy groups by the Sandmeyer reaction,[25,30] this strategy may be problematic for the bora-xanthone **4** due to the high reactivity of the triarylborane moiety. Therefore, we decided to prepare **4** from dichlorinated triarylborane **1** by a borylation and a subsequent oxidation of the boronic esters and benzylic moiety in a stepwise manner. Namely, the palladium-catalyzed borylation of **1a** with bis(pinacolate) diboron furnished diborylated **2a** in 61% yield. The selective oxidation of the two boronic esters in **2a** was accomplished by treatment with 2 equiv. of Oxone to yield the corresponding dihydroxy-substituted triarylborane **3a**. Further oxidation of **3a** with 2,3-dichloro-5,6-dicyano-*p*-benzoquinone (DDQ) in MeOH afforded boron-substituted dihydroxyxanthone **4** in 87% yield. After protecting the phenolic hydroxy groups in **4** with *t*-butyldimethylchlorosilane (TBDMSCl), the reaction with aryl Grignard reagents, followed by acidic workup with *p*-toluenesulfonic acid, finally produced bora-fluoresceins **BF1** and **BF2** as deep purple solids in 27% and 37% yield from **1a**, respectively.

This synthetic method was also applied for the preparation of *B*-phenyl-planarized bora-fluorescein **BF3**. 2,6-Di(2-propenyl) phenyl-substituted precursor **3b**, which was obtained by the method described above, was treated with $Sc(OTf)_3$ to promote a two-fold intramolecular Friedel–Crafts cyclization.[55] Using a procedure similar to that employed for the synthesis of **BF1** and **BF2**, albeit employing trimethylchlorosilane (TMSCl), *B*-phenyl-planarized **BF3** was obtained as purple solids in 9.8% yield from **1b**.

All bora-fluorescein derivatives are sufficiently stable to be handled under ambient conditions and can be purified by column chromatography on silica gel. However, in polar solvents such as acetonitrile, the color of *o*-tolyl-substituted **BF1** immediately changed from purple to yellow, while 2,6-dimethoxyphenyl-substituted **BF2** retained its purple color. This difference was confirmed by UV-vis absorption spectroscopy (Fig. S5, ESI†), which suggested that the discoloration of **BF1** in acetonitrile is mainly due to the coordination of a solvent molecule at the boron center (*vide infra*). Consequently, introduction of a proper aryl group at the 9-position of the fluorescein skeleton is essential to ensure the chemical stability of the **BF**s by suppressing undesired nucleophilic attacks not only at the 9-position but also at the boron center.

The structures of **BF2** and **BF3** were determined by single crystal X-ray diffraction analysis (Fig. 2). Although the crystal structure of **BF2** contains two crystallographically independent molecules in the unit cell, only one is shown in Fig. 2 as both are structurally similar. In both **BF2** and **BF3**, the boron atoms adopt a trigonal planar geometry with a C–B–C angle sum of 360°. The central six-membered rings that contain the boron atoms exhibit nearly planar geometries. The remaining two six-membered rings in the fluorescein skeleton adopt a coplanar conformation with dihedral angles of 4.7° (**BF2**) and 6.2° (**BF3**). These results suggest that the boron atom at the 10-position effectively participates in π-conjugation, irrespective of the sterics around the boron center. It is noteworthy that the fluorescein skeleton exhibits an unsymmetrical structure in the

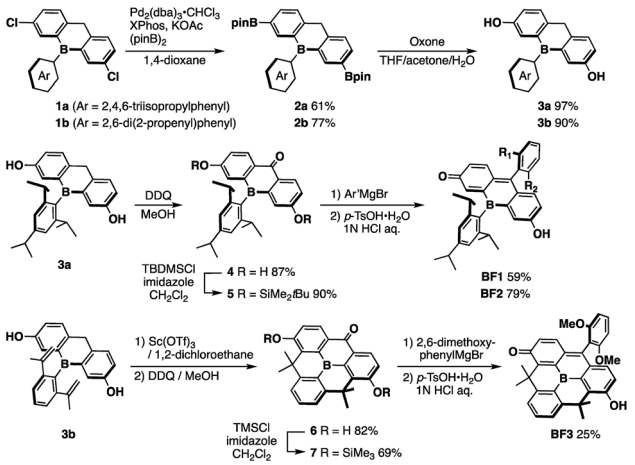

Scheme 1 Synthesis of bora-fluoresceins **BF1–3**.

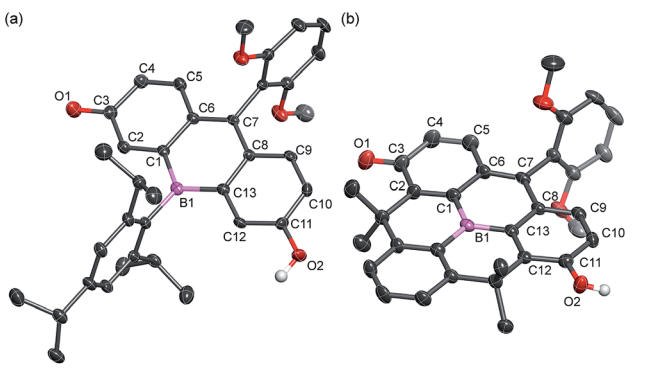

Fig. 2 Crystal structures of (a) **BF2** and (b) **BF3** (50% probability of thermal ellipsoids). Hydrogen atoms, except for those on the phenolic hydroxy groups, are omitted for clarity.

crystalline state. The six-membered C1–C6 ring adopts a quinoidal structure with marked bond alternation, while the other six-membered C8–C13 ring adopts a benzene-like structure. The unsymmetrical structures of **BF2** and **BF3** are probably due to crystal packing effects, *i.e.*, the formation of intermolecular hydrogen bonds between the hydroxy group in the phenol moiety of one molecule and the carbonyl group of the *p*-quinone methide moiety of an adjacent molecule (Fig. S1 and S3, ESI†).

Under basic conditions, bora-fluoresceins showed characteristic absorption and fluorescence in the NIR region (Fig. 3 and Table 1). **BF2** exhibited a broad absorption band with the maximum wavelength (λ_{abs}) of 538 nm ($\varepsilon = 0.84 \times 10^4\ M^{-1}\ cm^{-1}$) in acetonitrile. Upon addition of 1,8-diazabicyclo [5.4.0]undec-7-ene (DBU) as the Brønsted base to the acetonitrile solution of **BF2**, a significantly red-shifted absorption band emerged at $\lambda_{abs} = 851$ nm ($\varepsilon = 1.90 \times 10^4\ M^{-1}\ cm^{-1}$). This absorption band in the NIR region was attributed to the deprotonated form of **BF2**, which stems from the equilibrium at the phenolic hydroxy group. This notion is consistent with the behavior of other heteroatom-substituted fluorescein analogues, for which similar spectral changes have been observed (Fig. S7, ESI†). Under basic conditions, deprotonated **BF2** exhibited NIR fluorescence with the maximum at $\lambda_{em} = 907$ nm, while the fluorescence quantum yield is low ($\Phi_F = 0.003$).

A comparison of **BF2** with other heteroatom-substituted analogues clearly demonstrated the impact of the tricoordinate boron atom on the electronic structure. The λ_{abs} of **BF2** (851 nm in acetonitrile) under basic conditions is significantly red-shifted relative to those of the corresponding oxygen (**OF**: 524 nm; $\Delta\tilde{\nu} = 7330\ cm^{-1}$), dimethylsilyl (**SiF**: 612 nm; $\Delta\tilde{\nu} = 4560\ cm^{-1}$), and phosphine oxide (**POF**: 624 nm; $\Delta\tilde{\nu} = 3730\ cm^{-1}$) analogues. Meanwhile, the molar absorption coefficient of **BF2** ($\varepsilon = 1.90 \times 10^4\ M^{-1}\ cm^{-1}$) is about one-fifth that of **OF**, while their Stokes shifts are comparable. In the fluorescence spectra, deprotonated **BF2** exhibits the most red-shifted fluorescence in the NIR region, whereas **OF**, **SiF**, and **POF** only exhibit fluorescence in the visible-to-red region. It is noteworthy that the NIR absorption and fluorescence of **BF2** are even further red-shifted relative to those of the naphthofluorescein derivative **NAF D** (Fig. 1a), where the fluorescein skeleton is extended with two naphthalenes.[20] These comparisons clearly show that the tricoordinate boron atom significantly perturbs the electronic structure of the fluorescein skeleton.

Table 1 Photophysical properties of bora-fluoresceins and relevant analogues under basic conditions[a]

Dye	λ_{abs} [nm]	ε [$10^4\ M^{-1}\ cm^{-1}$]	λ_{em} [nm]	Stokes shift [cm^{-1}]
BF2	851	1.90	907	730
BF3	801	3.40	843	620
OF	524	9.95	544	700
SiF	612	12.3	627	390
POF	646	8.43	669	530
NAF D[b,c]	802	9.60	839	550

[a] Measured after addition of an excess amount of DBU in acetonitrile with a sample concentration of 1.2 to 3.2 $\times$ 10^{-5} M^{-1}. [b] Ref. 20. [c] Reported as a Cs salt in acetonitrile.

To elucidate the significant influence of the boron atom on the photophysical properties of the fluorescein dyes, the electronic structure of the deprotonated **BF2** was theoretically compared to those of **OF**, **SiF**, and **POF** by DFT calculations at the B3LYP/6-31+G(d) level of theory (Fig. 4). A remarkable difference was observed for their LUMO levels, where the specific orbital interaction between the fluorescein π-skeleton and the substituent at the 10-position plays a crucial role. **POF** has a low-lying LUMO due to the σ*–π* interaction between the P–Ph bond and the fluorescein skeleton, in addition to the inductive effect of the P=O moiety. Compared to the LUMO in **POF** that of **BF2** lies even lower by 0.23 eV. The low-lying LUMO level of **BF2** was attributed to the effective orbital interaction between the vacant p orbital on the boron atom and the π* orbital of the fluorescein skeleton. In contrast to the significant

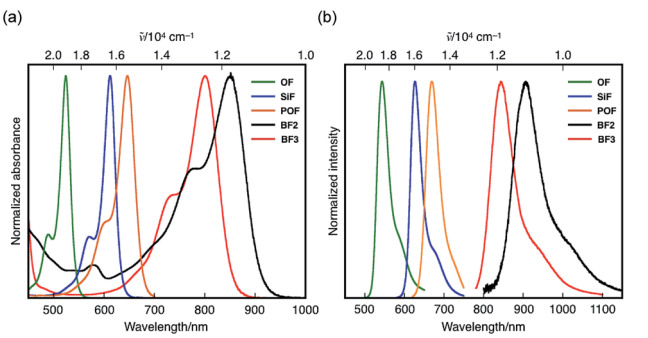

Fig. 3 (a) Absorption and (b) fluorescence spectra of heteroatom-substituted fluorescein dyes in the presence of DBU in acetonitrile.

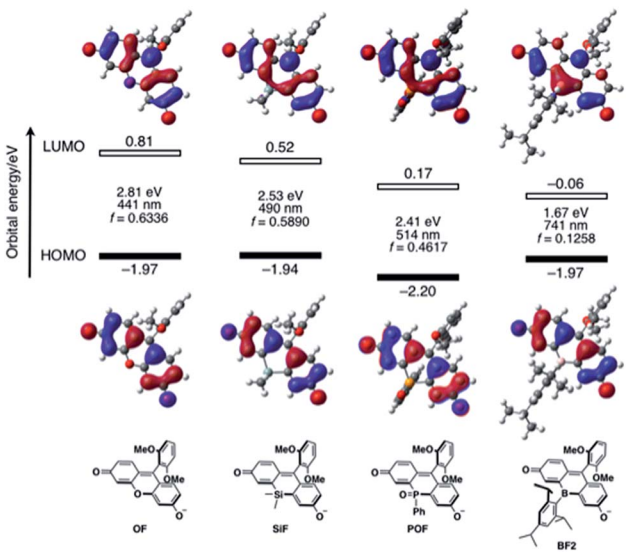

Fig. 4 Energy diagrams and Kohn–Sham plots of the HOMOs and LUMOs for the deprotonated forms of the fluorescein dyes **OF**, **SiF**, **POF**, and **BF2** calculated at the B3LYP/6-31+G(d) level of theory. The results of TD-DFT calculations at the same level of theory are also shown.

dependence of the LUMOs on the substituent at the 10-position of the fluorescein skeleton, the HOMOs are delocalized over the fluorescein skeleton with a node at the 10-position, regardless of the substituent. Consequently, **BF2** has a comparable HOMO level with those of the other analogues, except for **POF**, which has a slightly lower-lying HOMO due to the inductive effect of the P=O moiety. Overall, **BF2** exhibits the narrowest HOMO–LUMO gap in this series of fluorescein analogues.

TD-DFT calculations at the same level of theory suggested that deprotonated **BF2** exhibits a much red-shifted absorption maximum in the NIR region than the other fluorescein analogues (Fig. 4). The calculated oscillator strength for **BF2** is also significantly reduced compared to those of the other derivatives, which is consistent with the experimentally observed smallest molar absorption coefficient of **BF2**. This difference in the oscillator strength should be related to the contribution of the substituent at the 10-position to the LUMO, *i.e.*, the overlap between the HOMO and LUMO should decrease with increasing contribution of the substituent at the 10-position. Consequently, **BF2** has the smallest oscillator strength. Importantly, the narrow HOMO–LUMO gap observed in **BF2** is no longer retained once the vacant p orbital on the boron atom is occupied by a Lewis base externally added to form a tetracoordinate species (*vide infra*) (Fig. S14, ESI†). Therefore, only tricoordinate boron species that ensure the effective orbital interaction through the vacant p orbital on the boron atom can attain NIR-absorption and fluorescence.

The response to Lewis bases, such as fluoride ions, is a characteristic feature of boron-containing π-conjugated compounds, and should endow the bora-fluoresceins with unusual properties. Indeed, **BF2** exhibits drastic multi-stage color changes from purple to yellow and blue upon addition of tetra-*n*-butylammonium fluoride (TBAF). These color changes were monitored by UV-vis absorption spectroscopy. Upon addition of TBAF to an acetonitrile solution of **BF2** (2.8×10^{-5} M), the broad absorption band at $\lambda_{abs} = 538$ nm diminished with the concomitant emergence of a new absorption band at $\lambda_{abs} = 436$ nm (Fig. 5a). Successive addition of excess TBAF resulted in the appearance of an intense and sharp absorption band at $\lambda_{abs} = 585$ nm, which is reminiscent of the deprotonation of fluorescein dyes (Fig. 5b). Ultimately, the thus obtained mixture shows intense red fluorescence with the fluorescence maximum at $\lambda_{em} = 595$ nm with a high quantum yield of $\Phi_F = 0.89$.

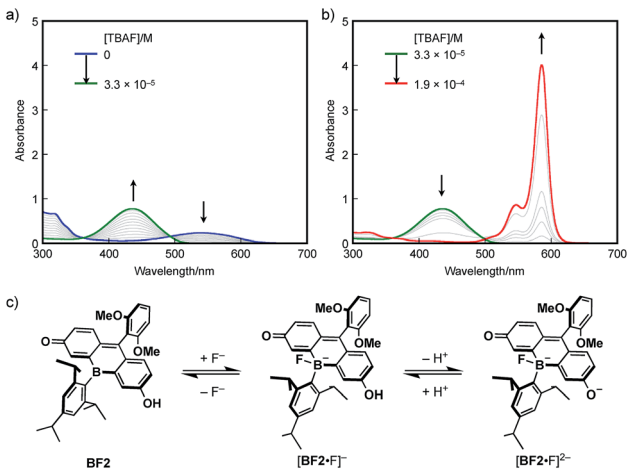

Fig. 5 UV-vis absorption spectral changes of **BF2** in acetonitrile (2.8×10^{-5} M) upon addition of TBAF: (a) [TBAF] = 0 to 3.3×10^{-5} M^{-1} and (b) 3.3×10^{-5} to 1.9×10^{-4} M^{-1}. (c) Equilibrium between neutral **BF2**, borate $[\mathbf{BF2}\cdot F]^-$, and borate fluorescein anion $[\mathbf{BF2}\cdot F]^{2-}$.

These changes can be interpreted in terms of a complexation of a fluoride ion at the boron center, followed by deprotonation of the phenolic hydroxy group in the fluorescein skeleton (Fig. 5c). Specifically, **BF2** initially incorporates a fluoride ion to form tetracoordinate borate $[\mathbf{BF2}\cdot F]^-$. With increasing TBAF concentration, subsequent deprotonation by the basic fluoride ion from $[\mathbf{BF2}\cdot F]^-$ generates borate fluorescein anion $[\mathbf{BF2}\cdot F]^{2-}$.[56–58] For a detailed study on the electronic structure of $[\mathbf{BF2}\cdot F]^-$ and $[\mathbf{BF2}\cdot F]^{2-}$, TD-DFT calculations were performed at the B3LYP/6-31+G(d) level of theory (Fig. S14, ESI†). The absorption bands observed at 436 nm for $[\mathbf{BF2}\cdot F]^-$ and 585 nm for $[\mathbf{BF2}\cdot F]^{2-}$ should be ascribed to π–π* transitions, which mainly consist of the HOMO–LUMO transitions in both complexes. It should be noted that the LUMOs of these complexes are delocalized over the fluorescein skeleton with a subtle contribution from the boron moiety, which stands in stark contrast to the orbital interaction observed in the LUMO of neutral **BF2** bearing a tricoordinate boron atom. Moreover, complexation with a fluoride ion switches the role of the boron moiety in the π-conjugated system from a π-electron-accepting unit to a strong σ-donating unit, giving rise to the red-shifted absorption of $[\mathbf{BF2}\cdot F]^{2-}$ compared to that of deprotonated **OF**. In this sense, the boron moiety in the fluorescein skeleton enables multi-stage electronic structure changes accompanied by drastic color changes in the visible-to-NIR region.

BF2 underwent complexation not only with fluoride ions, but also with weak neutral Lewis bases such as pyridine. It should be noted that in this case Lewis acid–base complexation predominates over the deprotonation of the phenolic hydroxy group (Fig. S11, ESI†). However, the binding constant of **BF2** with pyridine in acetonitrile is low ($K = 31$ M^{-1}) due to the steric congestion around the boron center induced by the bulky triisopropylphenyl group. In this context, we discovered that the Lewis acidity of the boron center was further enhanced by planarization of the *B*-phenyl group without the loss of chemical stability. Upon treatment of *B*-phenyl-planarized **BF3** with DBU in acetonitrile, deprotonated **BF3** showed red-shifted absorption at $\lambda_{abs} = 801$ nm, which is similar to the behavior of **BF2**. The hypsochromic shift of 730 cm^{-1} relative to the absorption of **BF2** (851 nm) is mainly due to the electron-donating effect of the methylene bridges in **BF3** (Fig. S13, ESI†). Deprotonated **BF3** exhibits NIR fluorescence ($\lambda_{em} = 843$ nm) with an improved fluorescence quantum yield ($\Phi_F = 0.03$). In contrast, upon treatment with pyridine, **BF3** showed a new hypsochromically shifted absorption band at 445 nm accompanied by a drastic color change from purple to yellow (Fig. S12, ESI†). On the basis of the UV-vis spectral changes, the binding constant of **BF3** toward pyridine was determined ($K = 2.1 \times 10^3$ M^{-1}), which indicated that the complexation ability of **BF3** toward pyridine is higher than that of **BF2** by two orders of magnitude.

Conclusions

In summary, we have successfully synthesized bora-fluoresceins **BF1–3**, which contain a tricoordinate boron atom at the 10-position in the fluorescein skeleton. The deprotonated forms of bora-fluoresceins exhibit absorption and fluorescence in the NIR region. In particular, deprotonated **BF2** shows absorption and emission maxima at 851 and 907 nm, respectively. These values are the most red-shifted of all hitherto reported heteroatom-substituted fluorescein dyes, demonstrating the significant impact of the boron atom on the electronic structure of fluorescein dye. The Lewis acidity of the boron atom offers a unique switching mechanism for the photophysical properties in addition to the Brønsted acid–base equilibrium on the fluorescein skeleton. Namely, the complexation of a Lewis base at the boron center of the bora-fluoresceins results in a significant hypsochromic shift of the absorption and emission. Consequently, bora-fluoresceins show multi-stage changes in their absorption and fluorescence properties, which is a noticeably different behavior from that of other heteroatom-substituted fluoresceins. The results of this study not only provide insight into the design principles of xanthene dyes, but also demonstrate the utility of tricoordinate boron atoms in the development of NIR dyes.

Conflicts of interest

There are no conflicts to declare.

Acknowledgements

This work was supported by JSPS KAKENHI grants 18H03909 and 18H05261. N. A. thanks the JSPS for a Research Fellowship for Young Scientists. The authors also thank Prof. Dr T. Sasamori (Nagoya City Univ.) and Dr M. Hirai (Nagoya Univ.) for their help with the X-ray crystallographic analysis. The synchrotron X-ray crystallography experiment was performed at the BL40XU beamline of SPring-8 with the approval of the Japan Synchrotron Radiation Research Institute (JASRI; proposal 2017B1179).

Notes and references

1 T. Terai and T. Nagano, *Curr. Opin. Chem. Biol.*, 2008, **12**, 515–521.
2 L. D. Lavis and R. T. Raines, *ACS Chem. Biol.*, 2008, **3**, 142–155.
3 H. Kobayashi, M. Ogawa, R. Alford, P. L. Choyke and Y. Urano, *Chem. Rev.*, 2010, **110**, 2620–2640.
4 X. Chen, T. Pradhan, F. Wang, J. S. Kim and J. Yoon, *Chem. Rev.*, 2012, **112**, 1910–1956.
5 J. Chan, S. C. Dodani and C. J. Chang, *Nat. Chem.*, 2012, **4**, 973–984.
6 H. Zheng, X.-Q. Zhan, Q.-N. Bian and X.-J. Zhang, *Chem. Commun.*, 2013, **49**, 429–447.
7 L. D. Lavis and R. T. Raines, *ACS Chem. Biol.*, 2014, **9**, 855–866.
8 X. Li, X. Gao, W. Shi and H. Ma, *Chem. Rev.*, 2014, **114**, 590–659.
9 J. Yin, Y. Hu and J. Yoon, *Chem. Soc. Rev.*, 2015, **44**, 4619–4644.
10 R. Weissleder, *Nat. Biotechnol.*, 2001, **19**, 316–317.
11 R. Weissleder and V. Ntziachristos, *Nat. Med.*, 2003, **9**, 123–128.
12 J. V Frangioni, *Curr. Opin. Chem. Biol.*, 2003, **7**, 626–634.
13 K. Kiyose, H. Kojima and T. Nagano, *Chem.–Asian J.*, 2008, **3**, 506–515.
14 L. Yuan, W. Lin, K. Zheng, L. He and W. Huang, *Chem. Soc. Rev.*, 2013, **42**, 622–661.
15 Z. Guo, S. Park, J. Yoon and I. Shin, *Chem. Soc. Rev.*, 2014, **43**, 16–29.
16 L. G. Lee, G. M. Berry and C.-H. Chen, *Cytometry*, 1898, **10**, 151–164.
17 K. Xu, B. Tang, H. Huang, G. Yang, Z. Chen, P. Li and L. An, *Chem. Commun.*, 2005, 5974–5976.
18 M. Sibrian-Vazquez, J. O. Escobedo, M. Lowry, F. R. Fronczek and R. M. Strongin, *J. Am. Chem. Soc.*, 2012, **134**, 10502–10508.
19 E. Azuma, N. Nakamura, K. Kuramochi, T. Sasamori, N. Tokitoh, I. Sagami and K. Tsubaki, *J. Org. Chem.*, 2012, **77**, 3492–3500.
20 K. Sezukuri, M. Suzuki, H. Hayashi, D. Kuzuhara, N. Aratani and H. Yamada, *Chem. Commun.*, 2016, **52**, 4872–4875.
21 J. Arden-Jacob, J. Frantzeskos, N. U. Kemnitzer, A. Zilles and K. H. Drexhage, *Spectrochim. Acta, Part A*, 2001, **57**, 2271–2283.
22 J. B. Grimm, A. J. Sung, W. R. Legant, P. Hulamm, S. M. Matlosz, E. Betzig and L. D. Lavis, *ACS Chem. Biol.*, 2013, **8**, 1303–1310.
23 K. Kolmakov, V. N. Belov, C. A. Wurm, B. Harke, M. Leutenegger, C. Eggeling and S. W. Hell, *Eur. J. Org. Chem.*, 2010, 3593–3610.
24 M. Fu, Y. Xiao, X. Qian, D. Zhao and Y. Xu, *Chem. Commun.*, 2008, 1780–1782.
25 T. Egawa, Y. Koide, K. Hanaoka, T. Komatsu, T. Terai and T. Nagano, *Chem. Commun.*, 2011, **47**, 4162–4164.
26 Y. Kushida, T. Nagano and K. Hanaoka, *Analyst*, 2015, **140**, 685–695.
27 T. Ikeno, T. Nagano and K. Hanaoka, *Chem.–Asian J.*, 2017, **12**, 1435–1446.
28 Y. Koide, Y. Urano, K. Hanaoka, T. Terai and T. Nagano, *ACS Chem. Biol.*, 2011, **6**, 600–608.
29 H. Nie, J. Jing, Y. Tian, W. Yang, R. Zhang and X. Zhang, *ACS Appl. Mater. Interfaces*, 2016, **8**, 8991–8997.
30 A. Fukazawa, S. Suda, M. Taki, E. Yamaguchi, M. Grzybowski, Y. Sato, T. Higashiyama and S. Yamaguchi, *Chem. Commun.*, 2016, **52**, 1120–1123.
31 X. Chai, X. Cui, B. Wang, F. Yang, Y. Cai, Q. Wu and T. Wang, *Chem.–Eur. J.*, 2015, **21**, 16754–16758.
32 X. Zhou, R. Lai, J. R. Beck, H. Li and C. I. Stains, *Chem. Commun.*, 2016, **52**, 12290–12293.
33 X. Chai, J. Xiao, M. Li, C. Wang, H. An, C. Li, Y. Li, D. Zhang, X. Cui and T. Wang, *Chem.–Eur. J.*, 2018, **24**, 14506–14512.

34 T. Hirayama, A. Mukaimine, K. Nishigaki, H. Tsuboi, S. Hirosawa, K. Okuda, M. Ebihara and H. Nagasawa, *Dalton Trans.*, 2017, **46**, 15991–15995.
35 M. R. Detty, P. N. Prasad, D. J. Donnelly, T. Ohulchanskyy, S. L. Gibson and R. Hilf, *Bioorg. Med. Chem.*, 2004, **12**, 2537–2544.
36 J. Liu, Y.-Q. Sun, H. Zhang, H. Shi, Y. Shi and W. Guo, *ACS Appl. Mater. Interfaces*, 2016, **8**, 22953–22962.
37 G. Dejouy, M. Laly, I. E. Valverde and A. Romieu, *Dyes Pigm.*, 2018, **159**, 262–274.
38 B. Calitree, D. J. Donnelly, J. J. Holt, M. K. Gannon, C. L. Nygren, D. K. Sukumaran, J. Autschbach and M. R. Detty, *Organometallics*, 2007, **26**, 6248–6257.
39 Y. Koide, M. Kawaguchi, Y. Urano, K. Hanaoka, T. Komatsu, M. Abo, T. Terai and T. Nagano, *Chem. Commun.*, 2012, **48**, 3091–3093.
40 M. W. Kryman, G. A. Schamerhorn, K. Yung, B. Sathyamoorthy, D. K. Sukumaran, T. Y. Ohulchanskyy, J. B. Benedict and M. R. Detty, *Organometallics*, 2013, **32**, 4321–4333.
41 M. W. Kryman, G. A. Schamerhorn, J. E. Hill, B. D. Calitree, K. S. Davies, M. K. Linder, T. Y. Ohulchanskyy and M. R. Detty, *Organometallics*, 2014, **33**, 2628–2640.
42 L. V. Lutkus, H. E. Irving, K. S. Davies, J. E. Hill, J. E. Lohman, M. W. Eskew, M. R. Detty and T. M. McCormick, *Organometallics*, 2017, **36**, 2588–2596.
43 N. Shimomura, Y. Egawa, R. Miki, T. Fujihara, Y. Ishimaru and T. Seki, *Org. Biomol. Chem.*, 2016, **14**, 10031–10036.
44 X. Zhou, L. Lesiak, R. Lai, J. R. Beck, J. Zhao, C. G. Elowsky, H. Li and C. I. Stains, *Angew. Chem., Int. Ed.*, 2017, **56**, 4197–4200.
45 C. D. Entwistle and T. B. Marder, *Angew. Chem., Int. Ed.*, 2002, **41**, 2927–2931.
46 C. D. Entwistle and T. B. Marder, *Chem. Mater.*, 2004, **16**, 4574–4585.
47 F. Jäkle, *Coord. Chem. Rev.*, 2006, **250**, 1107–1121.
48 S. Yamaguchi and A. Wakamiya, *Pure Appl. Chem.*, 2006, **78**, 1413–1424.
49 F. Jäkle, *Chem. Rev.*, 2010, **110**, 3985–4022.
50 A. Wakamiya and S. Yamaguchi, *Bull. Chem. Soc. Jpn.*, 2015, **88**, 1357–1377.
51 A. Escande and M. J. Ingleson, *Chem. Commun.*, 2015, **51**, 6257–6274.
52 Y. Ren and F. Jäkle, *Dalton Trans.*, 2016, **45**, 13996–14007.
53 L. Ji, S. Griesbeck and T. B. Marder, *Chem. Sci.*, 2017, **8**, 846–863.
54 E. von Grotthuss, A. John, T. Kaese and M. Wagner, *Asian J. Org. Chem.*, 2018, **7**, 37–53.
55 Z. Zhou, A. Wakamiya, T. Kushida and S. Yamaguchi, *J. Am. Chem. Soc.*, 2012, **134**, 4529–4532.
56 K. H. Lee, H.-Y. Lee, D. H. Lee and J.-I. Hong, *Tetrahedron Lett.*, 2001, **42**, 5447–5449.
57 H. Tong, G. Zhou, L. Wang, X. Jing, F. Wang and J. Zhang, *Tetrahedron Lett.*, 2003, **44**, 131–134.
58 D. A. Jose, P. Kar, D. Koley, B. Ganguly, W. Thiel, H. N. Ghosh and A. Das, *Inorg. Chem.*, 2007, **46**, 5576–5584.